AGU PUBLICATIONS

JGR

Journal of Geophysical Research: Solid Earth

RESEARCH ARTICLE
10.1002/2015JB012668

Key Points:
- SH wave reflection seismic resolves the first 400 m depth at high resolution in the Otway Basin
- SH wave seismic profiles detect present-day activity on the near-surface faults
- SH wave reflection seismic complements P wave reflection seismics

Correspondence to:
T. Beilecke,
thies.beilecke@bgr.de

Citation:
Beilecke, T., C. M. Krawczyk, J. Ziesch, and D. C. Tanner (2016), Near-surface fault detection using high-resolution shear wave reflection seismics at the CO2CRC Otway Project site, Australia, *J. Geophys. Res. Solid Earth*, *121*, 6510–6532, doi:10.1002/2015JB012668.

Received 17 NOV 2015
Accepted 23 JUL 2016
Accepted article online 28 JUL 2016
Published online 15 SEP 2016

Near-surface fault detection using high-resolution shear wave reflection seismics at the CO2CRC Otway Project site, Australia

Thies Beilecke[1,2], Charlotte M. Krawczyk[1,3,4], Jennifer Ziesch[1], and David C. Tanner[1]

[1]Leibniz Institute for Applied Geophysics, Hannover, Germany, [2]Now at Federal Institute for Geosciences and Natural Resources (BGR), Hannover, Germany, [3]Now at GFZ German Research Centre for Geosciences, Potsdam, Germany, [4]Now at Department of Applied Geosciences, Technische Universität Berlin, Berlin, Germany

Abstract High-resolution, near-surface, shear wave reflection seismic measurements were carried out in November 2013 at the CO2CRC Otway Project site, Victoria, Australia, with the aim to determine whether and, if so, where deeper faults reach the near subsurface. From a previous *P* wave 3-D reflection seismic data set that was concentrated on a reservoir at 2 km depth, we can only interpret faults up to 400 m below sea level. For the future monitoring in the overburden of the CO_2 reservoir it is important to know whether and how the faults continue in the subsurface. We prove that two regional fault zones do in fact reach the surface instead of dying out at depth. Individual first-break signatures in the shot gathers along the profiles support this interpretation. However, this finding does not imply perforce communication between the reservoir and the surface in the framework of CO_2 injection. The shear wave seismic sections are complementary to existing *P wave* volumes. They image with high resolution (better than 3 m vertically) different tectonic structures. Similar structures also outcrop on the southern coast of the Otway Basin. Both the seismic and the outcrops evidence the complex youngest structural history of the area.

1. Introduction

The subsurface structure and possible pathways in a region depend on the regional stress field and local conditions. While the exploration depth of a target defines the survey setup in general, it is also necessary to image subsurface pathways as a precondition to comprehend fluid migration processes for safe later use and geotechnical planning. In addition to the reservoir characteristics in the deeper subsurface, existing near-surface structures also play an important role. For instance, fault-bounded structures can provide possible pathways for CO_2 to enter groundwater aquifers.

To unravel the specific potential of communicating systems that occur between reservoir and surface in the framework of CO_2 injection, the joint project PROTECT (PRediction Of deformation To Ensure Carbon Traps) was initiated to assure long-term storage integrity and sensitive monitoring strategies, utilizing a special workflow [*Krawczyk et al.*, 2011, 2015]. To this end, PROTECT cooperates with CO2CRC Limited, Melbourne, Australia at the Otway Project site. An overview of the CO2CRC Otway Project is given by *Jenkins et al.* [2011] and *Cook* [2014].

Existing 3-D *P* wave reflection seismic data that cover the Otway Project site had been planned mainly to image deeper targets and therefore lacked near-surface resolution, impeding the imaging of faults that may reach all the way to the surface. *Spencer and La Pedalina* [2006], for instance, show a seismic cross section with a fault reaching up to ~200 m below sea level (bsl), just north of the site. *Ziesch et al.* [2015] predicted enhanced near-surface deformation in some areas based on the analysis of the existing Nirranda-Heytesbury 3-D seismic volume [*CGG Australia Pty. Ltd.*, 2000]. In these areas we acquired new 2-D shear wave seismic data (Figure 1).

The reason to use shear waves was based on the fact that these have proved able, in a number of settings, to image near-surface structures with a higher resolution than *P* waves [e.g., *Inazaki*, 2004; *Polom et al.*, 2010, 2013; *Pugin et al.*, 2013; *Krawczyk et al.*, 2013; *Malehmir et al.*, 2013]. Theoretically, in hard rock with a Poisson's ratio of 0.25, shear waves offer $\sqrt{3}$ times higher spatial resolution than *P* waves, if the same source signal frequencies are used, due to their slower propagation velocities. In a sedimentary environment, they typically

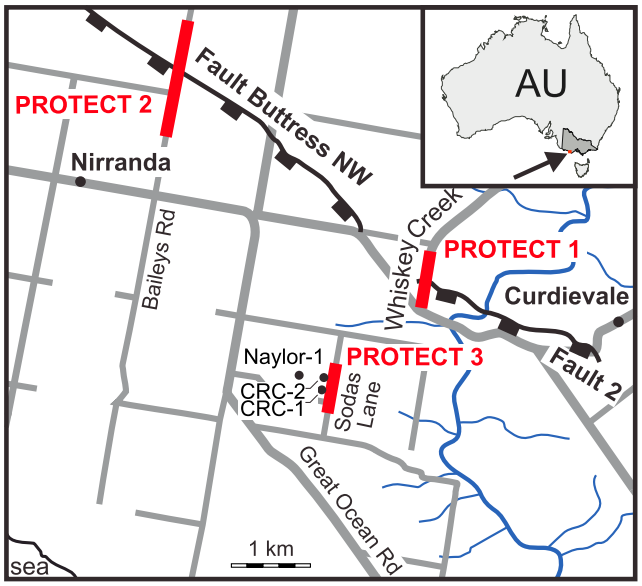

Figure 1. Locations of seismic profiles PROTECT 1–3 that cross surface extrapolations of fault zones Buttress NW and Fault 2 interpreted at depth. CRC-1 is the CO_2 injection well.

provide about twice the resolution of *P* waves [*Sheriff and Geldart*, 1995]. However, in unconsolidated units that are typically present in the near surface they can even offer more than 10 times the resolution [e.g., *Pugin et al.*, 2013; *Krawczyk et al.*, 2013; *Schön*, 2004, and references therein].

From the experience cited, such resolution increase was anticipated in the planning of the PROTECT survey, i.e., to image subtle structure details that were expected in the uppermost units and thus to offer an additional component for the determination of reservoir integrity and storage safety over the whole distance from reservoir to the surface. Apart from a higher spatial resolution the shear wave data also provide additional information for more detailed geomechanical parameter analysis, e.g., Poisson's ratio from Vp/Vs [e.g., *Beilecke et al.*, 2014a].

2. Geological Setting

The CO2CRC Otway Project site is situated in the Port Campbell Embayment of the Otway Basin on the south coast of Australia (Figure 1). The Otway Basin is a passive margin rift related to the Gondwana breakup and the separation of Australia and Antarctica [*Williamson et al.*, 1990]. The fault strike in the region is mainly NW-SE. The main normal fault dip direction is SW, with some related antithetic faulting. Detailed geological information about the Port Campbell Embayment is given by *Tickell et al.* [1992] and *Edwards et al.* [1994]. A recent study of the local subsurface fault kinematics with a compilation of the local geological evolution is provided in *Ziesch et al.* [2015].

A number of reports show that the passive margin setting in the Otway Basin has not been a strictly normal fault setting over time. During Middle to Late Jurassic, inversion took place, and during the Miocene, inversion began again, causing reverse faulting and folding, which is still ongoing [*Norvick and Smith*, 2001]. The compressional regime and associated inversion show distinct phases [e.g., *Holford et al.*, 2014, and references therein]. The authors relate periods of compressional activity to changes in the intraplate stress regime, resulting from significant modifications in the movements of one or more plate boundary segments. Even subtle compressional features, independent of the eustatic evolution, can be identified on the surface as offset strandlines [*Wallace et al.*, 2007]. Minor dextral strike-slip fault behavior of the Otway Basin has been reported by *Perincek and Cockshell* [1995]. By analyzing fault surface topography, *Ziesch et al.* [2015] show that 40% of the normal faults possess a local dextral strike-slip component.

The CO_2 storage site is located in the Naylor gas field, which was described in *Vidal-Gilbert et al.* [2010]. Storage is in the late Cretaceous Waarre Formation that has been proven to be able to hold a methane-rich gas accumulation over geological timescales. The Naylor field is bound to the west by the north-south trending normal

Table 1. Near-Surface Stratigraphic Model at Naylor-1 Well[a]

Formation	Depth below surface (m)
Soil	0–0.5
Clay, dry	0.5–4.0
(Port Campbell) Limestone	4.0–122.0
Gelibrand Marl	122.0–457.0
Clifton Formation	457.0–474.0

[a]After *Al-Jabri and Urosevic* [2010].

Naylor Fault. According to *Vidal-Gilbert et al.* [2010], its throw is too small to compromise the seal integrity of the Belfast mudstone seal formation above it. In a 3-D *P* wave data set the throw is estimated to be 225 m. This fault is thought to be the reservoir pivot because it marks the boundary in the updip direction. To the east, the Naylor structure is cut by the normal Naylor East Fault and is bound to the south by the Naylor South Fault. The latter two faults are not expected to coincide with the path of the injected CO_2 plume.

Most important for the shear wave survey is the near-surface geology. The uppermost units above the Narrawaturk Marl are, from oldest to youngest, the Clifton Formation, the Gelibrand Marl, and the Port Campbell Limestone. These formations were deposited in an increasingly shallow marine setting with increasing calcarenite components. Units along the coast [*Tickell et al.*, 1992; *Edwards et al.*, 1994] often show karst structures that pose risk to near-surface construction works [*Whiteley*, 2012]. The top layer is made up of the Hanson Plain Sand that represents the most recent sediments after the latest uplift. According to *Tickell et al.* [1992], it hampers the ingress of water to deeper levels and its thickness thus defines the occurrence of sinkholes in the area.

Detailed information regarding the stratigraphic formations are given in, e.g., *Edwards et al.* [1996], via the Australian Stratigraphic Units Database [*Geoscience Australia*, 2015], and in *Ziesch et al.* [2015]. A simple near-surface stratigraphic model near the Cooperative Research Centre (CRC) boreholes—inferred from the Naylor-1 well—is provided in Table 1. Additional stratigraphic information in the vicinity of the Otway Project site is provided by the Victorian Department of Environment, Land, Water and Planning on their website (Table 2 [*State of Victoria*, 2015]).

Other sources of near-surface stratigraphy are sparse. Even though, e.g., *Schacht et al.* [2011] and *Hortle et al.* [2011] report groundwater analyses from a number of boreholes in the area, they do not report stratigraphic details.

3. Shear Wave Reflection Seismic Surveying

In November 2013, we carried out a 2-D shear wave seismic survey at the CO2CRC Otway Project site. The shear wave measurements were conducted at locations where known fault zones in a 3-D seismic volume at larger depth (> 400 m) [*Ziesch et al.*, 2015] would intersect the surface, if the faults dipped at the same angle as they do at depth. An illustration of fault zones in the vicinity of the site is given in Figures 2 and 3. These sections from the Nirranda-Heytesbury 3-D *P* wave seismic cube show a typical synsedimentary passive margin setting.

Table 2. Groundwater Bore Information[a]

Layers	Location Nirranda South (m)	Location Nullawarre (m)
Upper Tertiary Sand	0–3	0–3
Upper mid-Tertiary: fractured limestone, sand, gravel, clay, and minor coal	3–140	3–253
Upper Mid-Tertiary: clay, silt, fractured marl, and minor sand	140–487	253–608

[a]Values in meters below surface [*State of Victoria*, 2015].

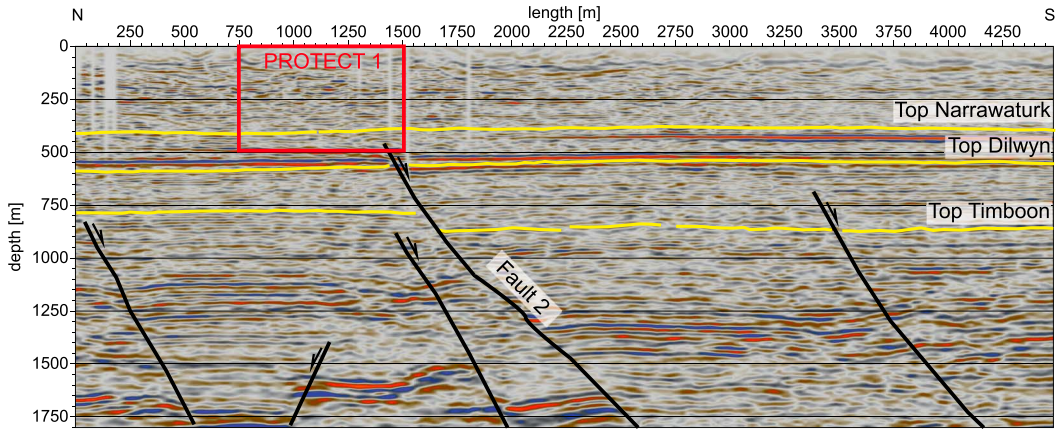

Figure 2. The 4.5 km long and 1.8 km deep 2-D cross section through the Nirranda-Heytesbury 3-D *P* wave seismic cube [*CGG Australia Pty. Ltd.*, 2000], showing *SH* wave profile PROTECT 1. Due to sparse near-surface resolution, units above Top Narrawaturk and any possible upward continuation of fault zones cannot be interpreted.

The *P* wave data were mainly acquired with vibrator sources with frequencies up to 90 Hz. Importantly, the field layout utilized source and receiver arrays of 40 m length at each station. Therefore, near-surface resolution is limited and the uppermost horizon that can be identified in these sections is the Top Narrawaturk. The paths of shear wave profiles PROTECT 1 and 2 were chosen to cross Fault 2 and Buttress NW [*Ziesch et al.*, 2015], as perpendicular as possible to their strikes. PROTECT 3 was carried out to image the subsurface in the direct vicinity of the CO2CRC wells (Figure 1).

The field setup of the shear wave survey consisted of an established system that comprised the hydraulic horizontal vibrator source MHV4S of Leibniz Institute for Applied Geophysics, Hannover, Germany (LIAG), with a Pelton Vib Pro control unit and a geophone streamer with 1 m geophone spacing. Source and receivers were run in *SH* orientation, i.e., particle motions perpendicular to the spread orientation [e.g., *Polom et al.*, 2010; *Krawczyk et al.*, 2013]. In this case a spread length of 240 m was used to constrain a deeper-reaching seismic velocity model than in the latter two citations. Mainly as a budget decision, shot point spacing was set to 4 m. During most of the survey, the source signal was a 12 s linear sweep of 20 to 100 Hz and 3 s listening time. At each shot point two sweeps with opposite polarity were used, first to suppress contaminating residual *P* wave signals and second to increase the signal-to-noise ratio. In addition to the geophone channels, we also recorded the nominal sweep signal, the ground force calculated by the vibrator control unit, and the data from two accelerometers on the vibrator unit with a Geometrics Geode seismograph system. Each sweep was

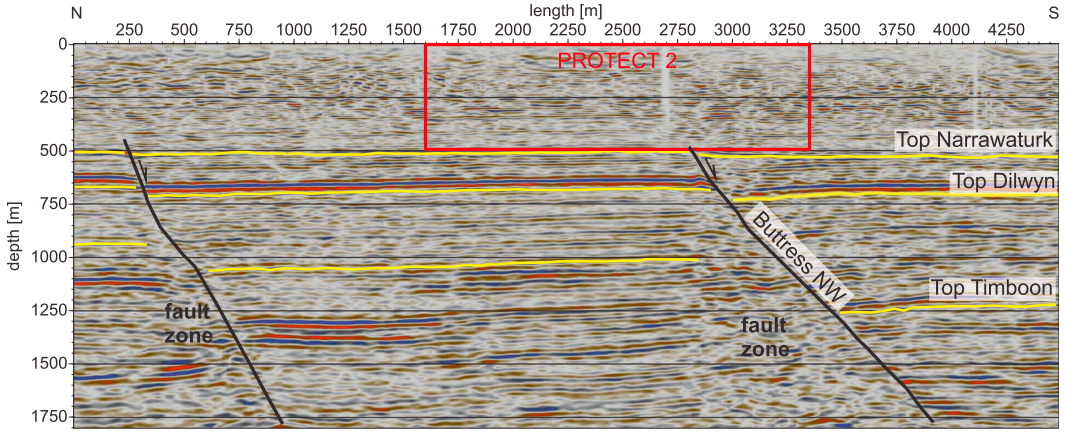

Figure 3. The 4.5 km long and 1.8 km deep 2-D cross section through the Nirranda-Heytesbury 3-D *P* wave seismic cube [*CGG Australia Pty. Ltd.*, 2000], showing *SH* wave profile PROTECT 2. Due to sparse near-surface resolution, units above Top Narrawaturk and any possible upward continuation of fault zones cannot be interpreted. Units below fault Buttress NW below a depth of ~1200 m are so strongly disturbed that unit interfaces cannot be identified. This way, Buttress NW rather defines a zone that is influenced by the fault.

Table 3. Main Shear Wave Survey Parameters

Parameter	Value
Survey type	shear wave
Survey orientation	*SH*
Signal source	hydraulic MHV4s of Leibniz Institute for Applied Geophysics (LIAG)
Source vehicle mass	3 t
Source control	Pelton Vib Pro
Source point spacing	4 m
Source pattern	none
Source signal	sweep
Number of sweeps per point	2 (opposed polarity)
Sweep frequency band	20–100 Hz linear
Sweep duration	12 s
Sweep tapers	0.5 s cosine
Geophone type	Sensor SM 6, horizontal, 10 Hz, 375 Ω
Geophone spacing	1 m
Geophone pattern	none
Spread length	240
Spread type	split spread
Recording unit	Geometrics Geode
Sample rate	2 ms
Antialias filter	208 Hz
other frequency filters	off
Gain	24 dB
Listening time	3 s

recorded without correlation with a sample rate of 2 ms. This setup resulted in a nominal spatial fold between 20 and 40 in the main parts of the profiles. The main survey parameters are summarized in Table 3.

Figure 4 sketches the acquisition geometry in the field. At the beginning and end of each profile the source gradually moved into and out of the asymmetric split-spread layout, respectively. The maximum offsets along most parts of the profiles thus were between 80 m and 160 m. The maximum source-to-receiver offset at the line ends was 240 m.

Weather conditions varied during data acquisition. A couple of days were warm (above 30°C) and almost windless, but most of the fieldwork took place under cool (around 15°C) and windy conditions. Since horizontal-component geophones are more wind-prone than vertical-component geophones, we tried to avoid measuring during gusts of wind. This strategy, the statistical advantage of 12 s sweep length, and the relatively high trace fold minimized the wind noise impact on the final results.

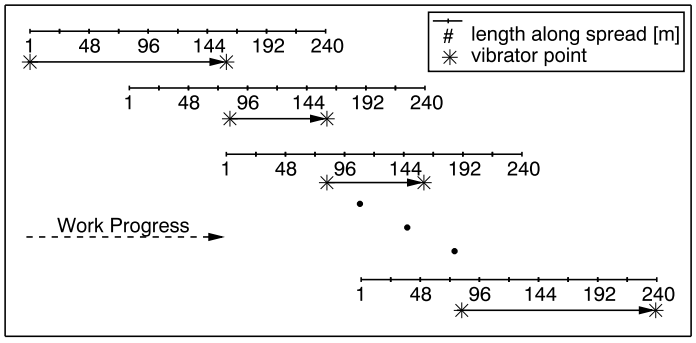

Figure 4. Acquisition geometry and working scheme of shear wave reflection seismic surveying in the Otway Basin.

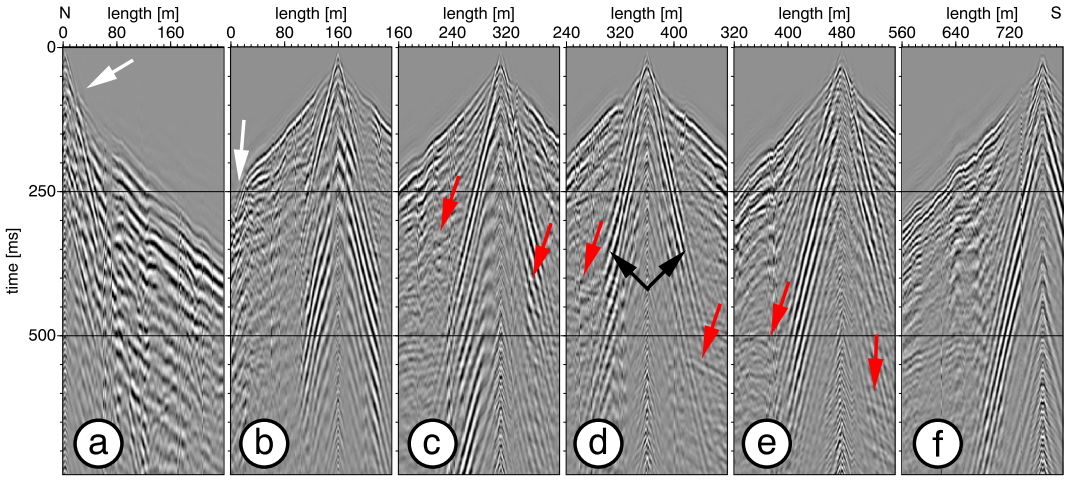

Figure 5. Shots along profile PROTECT 1. Surface wave onsets are indicated exemplarily with black arrows and dipping onsets with red arrows. (a) The northernmost shot and (a and b) the northernmost geophones are more strongly attenuated than (c–f) the ones along the rest of the profile, and their seismic signal has less bandwidth and lower direct wave velocities (white arrows).

The field-correlated data on the screen during data acquisition were often difficult to interpret in terms of recognizable reflection onsets due to strong surface wave signal pollution. However, the surface waves showed little dispersion and therefore could be easily removed during subsequent data processing. Examples of shots along profiles PROTECT 1 and 2 after correlation and vertical (shot point) stacking are depicted in Figures 5 and 6. The labeling of the geophone traces in the two figures represents their locations along either profile.

Surface waves are present in almost all of the depicted shot sections (black arrows), no matter whether the data were acquired on an asphalt road (PROTECT 1, Figure 5) or on a gravel road (PROTECT 2, Figure 6). In many of the shot sections along both profiles the first-break onsets show some undulations (white arrows) that can be attributed to variations in the weathering layer. In some of the sections, dipping events can be identified (red arrows). Clear reflection hyperbolas off the stratigraphic horizons are not always visible (Figures 5a, 6c, and 6d).

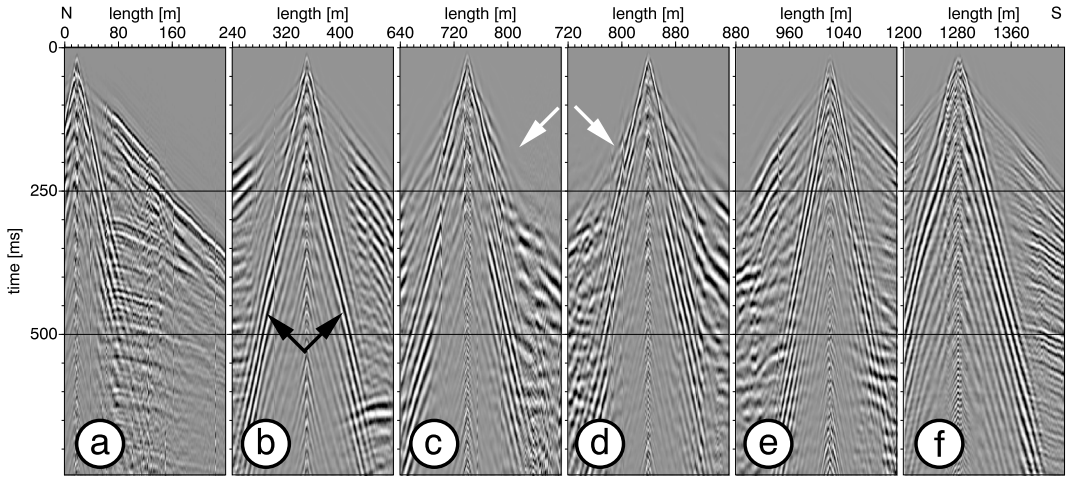

Figure 6. Shots along profile PROTECT 2. Surface wave onsets are indicated exemplarily with black arrows. (b–e) Shots located in the center of the profile are more strongly attenuated than (a and f) the ones at the profile tails, and their seismic signal has less bandwidth and lower direct wave velocities (white arrows).

Table 4. Shear Wave Processing Parameters

Processing Step	Application
Data load	SEG2-data load to ProMAX
Geometry setup	0.5 m bin interval
Vibroseis correlation	using individual sweeps, without previous noise filtering
Vertical stacking of records	twofold with opposed polarity
Editing	killing of bad traces could be neglected
Refraction statics	calculated from first-break picks with diminishing residual matrices (DRM), using replacement velocity of 790 m/s
Spectral balancing	11 panels 20–100 Hz
fk Filtering	arbitrary polygon
Velocity analysis	iterative interactive NMO, DMO, and inverse NMO strategy
Trace muting	stretch mute of 20% and muting of near offsets up to 20 m
Residual statics	not applied
Prestack Kirchhoff time	smoothed velocity field; top mute
Migration	by applying NMO stretch mute and inverse NMO on gathers
Time-to-depth conversion	average 1-D velocity
Scaling	spherical divergence, trace normalization, and 99% amplitude percentile

4. Data Processing

Data processing was carried out with the software ProMAX. The processing sequence and some basic parameters are summarized in Table 4. In the prestack domain, spectral balancing, subsequent fk filtering, and refraction statics were crucial steps that are in part different from the first processing approach reported in *Beilecke et al.* [2014b]. Additional predictive deconvolution tests were not successful.

Figures 5 and 6 represent shot sections before signal enhancement. After the application of refraction static correction, spectral whitening, and fk filtering, the corresponding shots are depicted in Figures 7 and 8. Note that surface wave arrivals are removed to a large degree (black arrows) and that reflection hyperbolas do not differ as much among the different shot sections of the respective profiles. Also, note that undulations along the first-break onsets are reduced (white arrows). The dipping onsets are still present in the sections (red arrows). Note that the northernmost shot along PROTECT 1 (Figure 7a) and the central shots along PROTECT 2 (Figures 8c and 8d), even after preprocessing, still show very few interpretable onsets.

P wave contamination in the single shot recordings was negligible. Therefore, it was not possible to successfully carry out vertical stacking of the two opposed-polarity shots at each shot point using the identical polarity, in order to gain *P* wave sections.

The statics' correction method we applied is the diminishing residual matrices method (DRM) [*Gulunay*, 1985], because it showed better results than the delay time method (DLT) [*Lawton*, 1989; *Hollingshead and Slater*, 1979] or the generalized reciprocal method (GRM) [*Palmer*, 1980, 1986]. In most cases, the first break was easy to pick because the ringiness of the signal was small.

The interval velocities we encountered at the Otway site were so fast that the apparent velocity difference between surface waves and reflections was large. This explains the success of the fk filter process on our data.

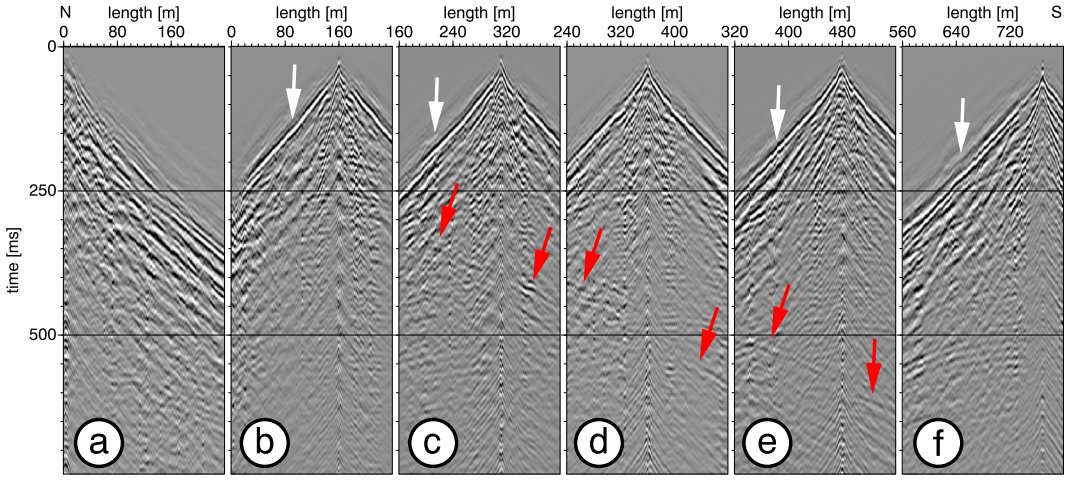

Figure 7. Shots along profile PROTECT 1. After data processing, surface wave onsets are removed to a large degree, first breaks better line up than in Figure 5 (white arrows, exemplarily), and reflection signatures are more similar among the different shots. Also, note that dipping onsets are still present (red arrows, exemplarily). (a–f) Same with Figures 5a–5f.

Also characteristic of the data, with respect to successful fk filtering, was the small amount of wave dispersion in the used signal frequency range of 20–100 Hz.

As opposed to refraction statics, the application of reflection residual statics' correction degraded the output insofar as steps along reflections in the final migrations became blurred, even though the determined static values were just on the order of a few milliseconds. Therefore, we decided to leave this step out of the processing scheme.

Velocity determination was carried out iteratively from the interactive analysis of Common Midpoint (CMP) gathers. The velocities were determined including Dip Moveout (DMO) to better focus semblance values in the velocity gathers [e.g., *Deregowski*, 1986; *Yilmaz*, 2001]. Traces within the offset range 0 to 20 m around the shot points had to be left out of the imaging and stacking process, because of signal distortion near the source related to filter noise after surface wave removal. This hampers the possible imaging of structures at the very near surface.

An example of a final stack of profile PROTECT 2 is shown in Figure 9. The northern and southern ends are dominated by horizontal reflections that can be associated with reflections off the sedimentary horizons,

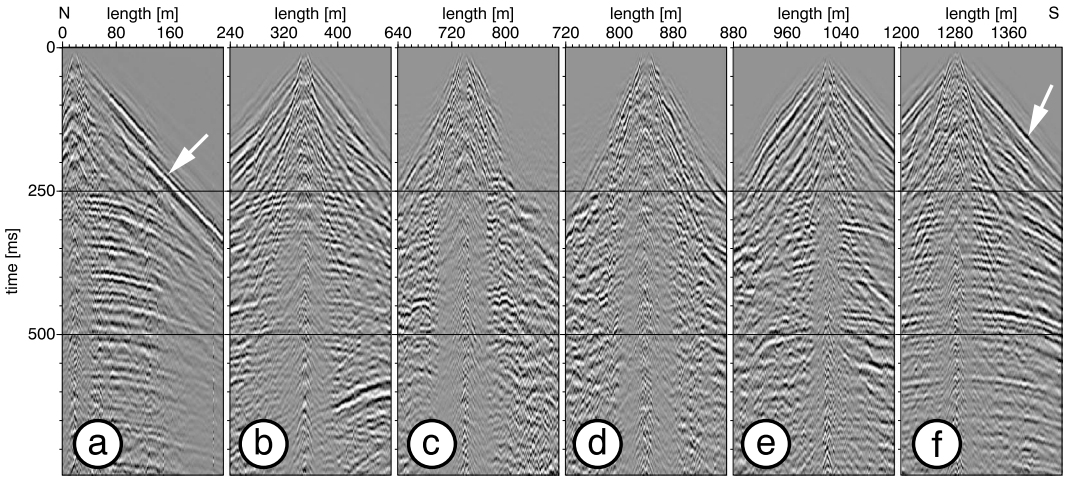

Figure 8. Shots along profile PROTECT 2. After data processing, surface wave onsets are removed to a large degree, first breaks better line up than in Figure 6 (white arrows, exemplarily), and reflection signatures are more similar among (a, b, e, and f) the shots, except for (c and d) the central shots.

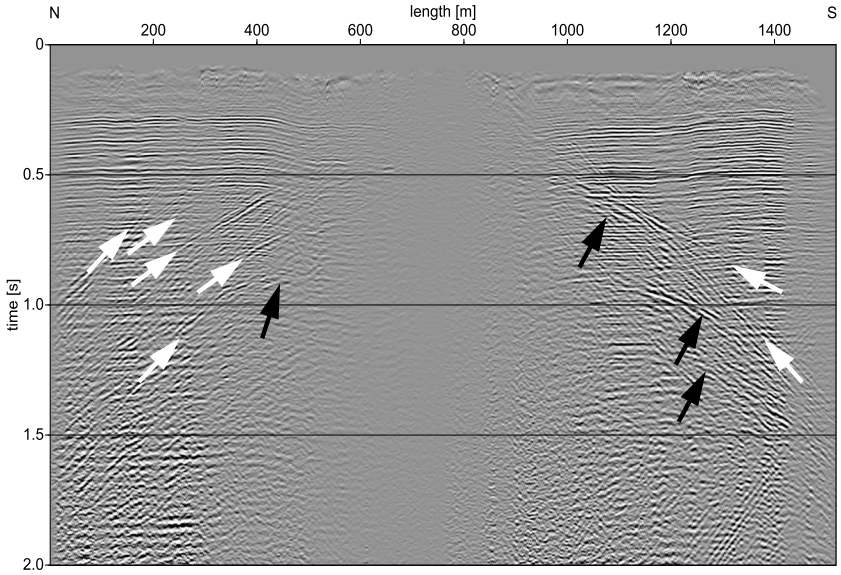

Figure 9. DMO stack of shots along profile PROTECT 2, plotted with spherical divergence correction of $t^{2.5}$ to 2 s traveltime, without subsquent trace normalization. Note that the reference datum of the section is above the ground level, i.e., 65 m above sea level (asl). White arrows indicate some of the linear onsets, and black arrows indicate some diffractions.

whereas in the central third of the stack very little signal is present. Note that the stack is plotted with spherical divergence amplitude control. If Automatic Gain Control (AGC) or subsequent trace normalization had been used, this part of the section would mainly show discontinuous and chaotic onsets.

In addition to the horizontal reflections, crosscutting dipping onsets can be identified. In the northern third, they are northward dipping with variable dips and curvature; in the southern third of the profile they are southward dipping with variable dips and curvature. In the latter part, more of the events show a diffraction shape. Even with AGC, a continuation of the diffraction onsets would not be detectable in the central part of the section.

The many differently dipping events in the stack led to the decision to carry out prestack time migration as a less compromising migration approach to DMO stacking and poststack time migration, since prestack time migration is the more rigorous method to avoid destructive interference of conflicting dips before the migration process [*Yilmaz*, 2001]. In fact, the prestack migrations show more details and higher resolution compared with DMO-stacked and postack-migrated sections. For prestack time migration, the same velocities were used that had been determined for stacking and poststack migration. Therefore, the final processing steps were prestack time migration and 1-D depth conversion, the latter with an average velocity model along each profile.

Often, the maximum shot-to-receiver offset is regarded as the maximum depth of a sufficiently constrained seismic interval velocity model. However, this assumption is for *P* waves; shear waves show larger moveouts. Therefore, it can be expected that a shear wave model is well constrained to deeper levels. As there was no indication of any shear wave anomalies with depth in the upper 500 m, the determined velocity trend from the upper units was extrapolated to greater depth for migration and depth conversion. Therefore, we believe that the determined velocities are well enough constrained for our purposes to at least 300 m, provided reflections could be used as reference, which was of course difficult in the central part of profile PROTECT 2. The determined shear wave stacking velocities transposed into interval velocities with Dix's conversion [*Dix*, 1955], are depicted in Figure 10. Even though a smoothed velocity field was used for migration, the step functions resulting from the Dix's conversion offer a better estimate of the quality of the determined velocities.

Apart from some local outliers, the basic velocity trend with depth goes from roughly 550 m/s at the very near surface to roughly 750 m/s immediately below, stays in the range 800 to 1000 m/s down to ~300 m, and basically stays below 1100 m/s above 500 m depth. This trend is similar for the other two PROTECT profiles. Even though it is tempting to use this velocity profile for structural interpretation, it is not well suited for such

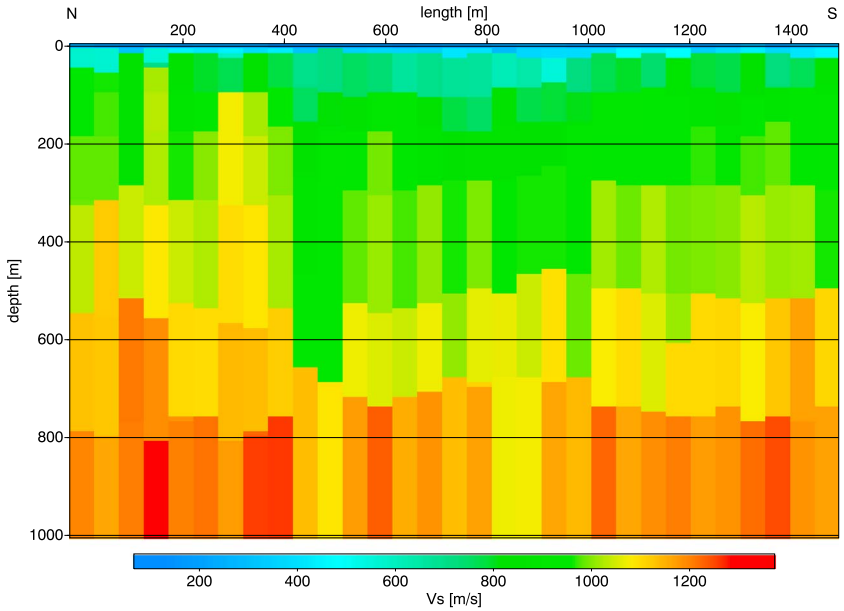

Figure 10. Shear wave interval velocities with depth calculated from determined stacking velocities with Dix's conversion [*Dix*, 1955] along profile PROTECT 2. Note that the lower parts of the profile are less well constrained than the upper parts. Also, note that the reference datum in this image is 65 m above sea level. For migration, a horizontally and vertically smoothed version of this velocity profile was used.

purpose. Any interpretation would be speculative. Reflection tomographically determined velocity models, which we do not have yet, would better serve such purpose.

Based on *Kallweit and Wood* [1982], the maximum spatial resolution of the data can be estimated using the highest frequency present in the data, under the assumption of a zero-phase wavelet, which is a valid assumption for a correlated sweep. If the refractor velocity of roughly 800 m/s along most parts of the profiles down to ~300 m and the maximum signal frequency of 100 Hz is presumed, the shortest wavelength we were able to accomplish is ~8 m, resulting in a vertical resolution of 2 m at best. According to *Sheriff and Geldart* [1995], the highest horizontal resolution can be estimated as double the vertical resolution after migration, if errors of typically 5% in the velocity model are considered. This means ~4 m horizontal resolution at best in our case. However, such an estimate is not valid in all of the sections, because depending on travel distance of the signal, higher frequencies are increasingly attenuated and velocities typically increase with depth, as can be seen in Figure 10. The vertical and horizontal resolution at larger depth therefore is smaller, even in areas of undisturbed rock units along the profiles.

5. Structural Architecture of the Upper 500 m Subsurface

For the presentation of the results gained by shear wave seismic imaging, we will show in the following the cross sections of shear wave profiles PROTECT 1–3 in gray scale in combination with the corresponding *P* wave sections, selected from the Nirranda-Heytesbury 3-D seismic cube at sea level datum, and color coded. The interpretation of the *P* wave data is taken from *Ziesch et al.* [2015], as indicated in Figures 2 and 3. The more detailed interpretations of the shear wave sections are then presented together with surface elevation and refractor properties. Thus, Figures 11 and 12 represent profile PROTECT 1, Figures 13 and 14 represent PROTECT 2, and Figures 16 and 17 represent PROTECT 3. This procedure best exhibits the different characters of the 3-D *P* wave and 2-D *S* wave surveys.

5.1. Profile PROTECT 1

Profile PROTECT 1 cuts across the possible extension of Fault 2 (for location, see Figure 1). The interpretation of the regional 3-D data set indicates the termination of this deeply reaching normal fault at ~400 m below sea level, close to the top Narrawaturk Formation (Figures 2 and 11 [*Ziesch et al.*, 2015]). Extrapolation of the fault from this point to the surface with the same fault dip predicts an intersection with the surface approximately in the southern third of profile PROTECT 1 (Figures 2 and 11, top).

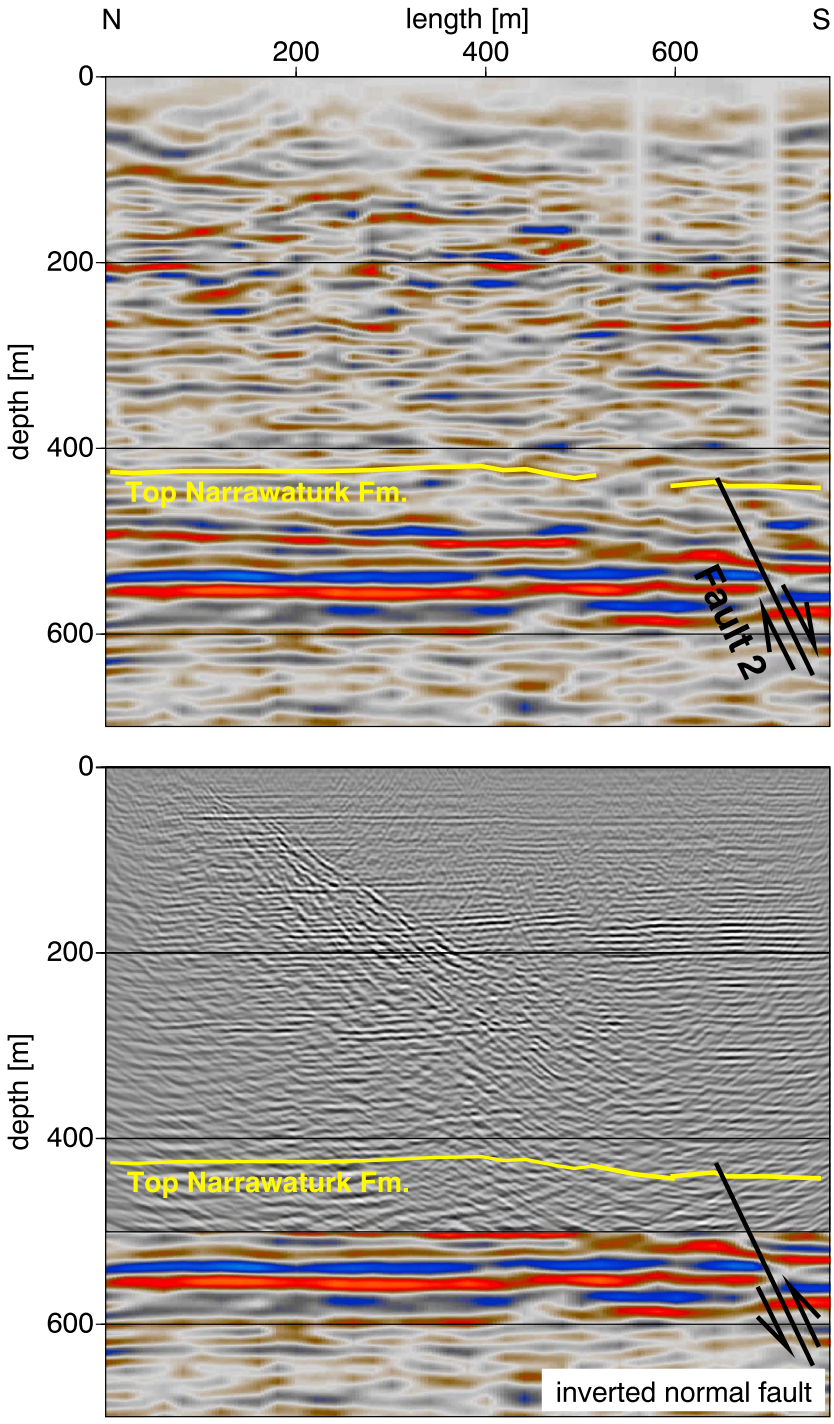

Figure 11. Cross sections along profile PROTECT 1. (top) *P* wave section from seismic cube Nirranda-Heytesbury 3-D at sea level datum with interpretation [*Ziesch et al.*, 2015]. (bottom) Shear wave cross section overlain.

Comparing the upper 500 m of the subsurface structure along the profile with respect to *P* wave (Figure 11, top) and newly acquired shear wave data (Figure 11, bottom), a far higher reflector resolution of the shear wave section is apparent. In addition, a remarkable group of reflectors dip from north to south at ~30° (Figure 11, bottom, from surface down to ~350 m depth). This adds structural detail that cannot be recognized in the *P* wave section. Structures deeper than 350 m are more difficult to interpret because shear wave signals at deeper levels are less clear and therefore offer less resolution.

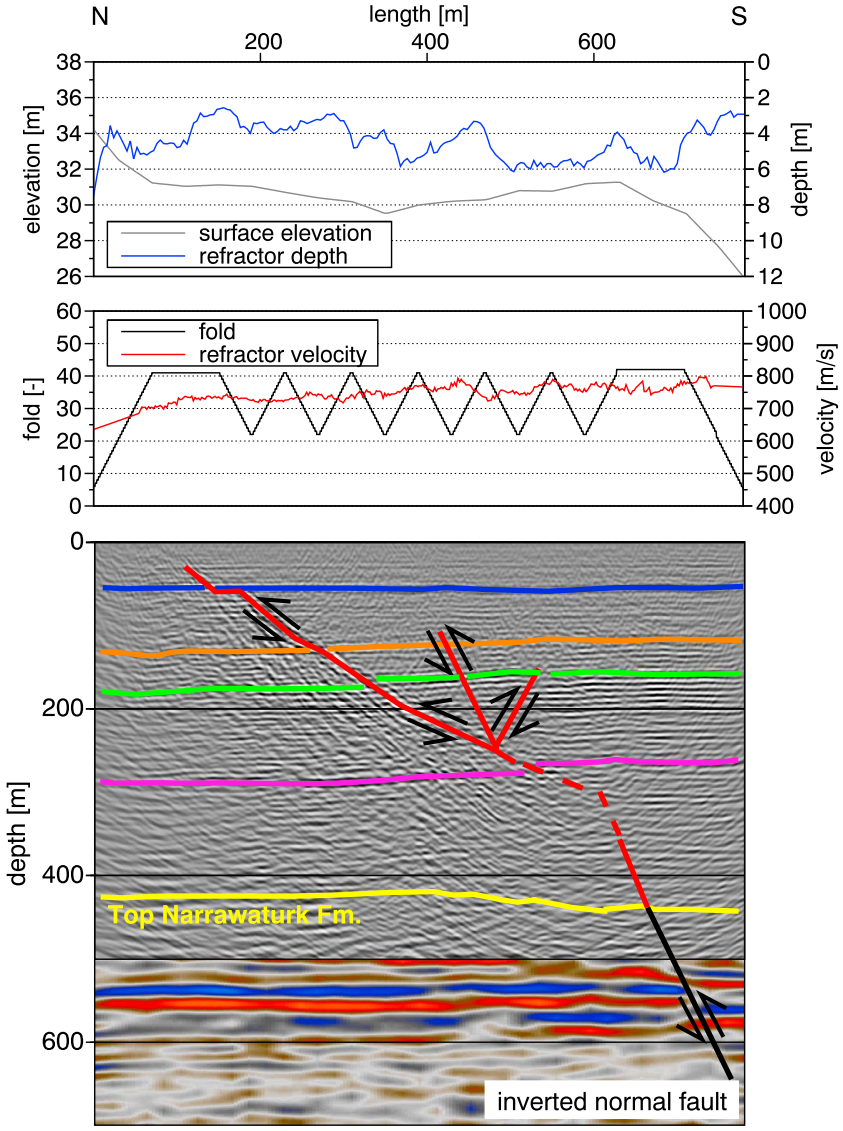

Figure 12. Detailed structure of PROTECT 1. (top) Surface elevation and refractor properties from the shear wave data. (bottom) Interpretation of the high-resolution shear wave image at sea level datum. The horizon marked in green shows a throw of at least 2 m.

We interpret that the dipping events mark reflections of details of an incipient thrust (reverse fault) propagating upward (Figure 12, bottom). We also suggest that this fault is connected to the normal fault at 300–350 m depth, meaning that the normal fault has been inverted. Note that the interpreted fault shows some steps. Throw of the reflector geometries across the interpreted fault surfaces can be measured with high resolution. For instance, the horizon marked in light green color above the 200 m depth line has an interpretable throw, which means according to our estimate 2 m or somewhat more (Figure 12, bottom).

The surface topography (Figure 12, top) corroborates this fault interpretation. If the two minor faults in the center of the profile are extrapolated to the surface, they end at small topographic highs at profile lengths of 350 m and 620 m. An even larger surface expression of the reverse fault zone is the elevation increase at the northern end of the profile. The existing hillside would thus represent a tectonic feature, related to the reverse fault zone, possibly a hanging wall anticline. In contrast, refractor depth and refractor velocity along this profile do not show any first-order, fault-related anomalies (Figure 12, top).

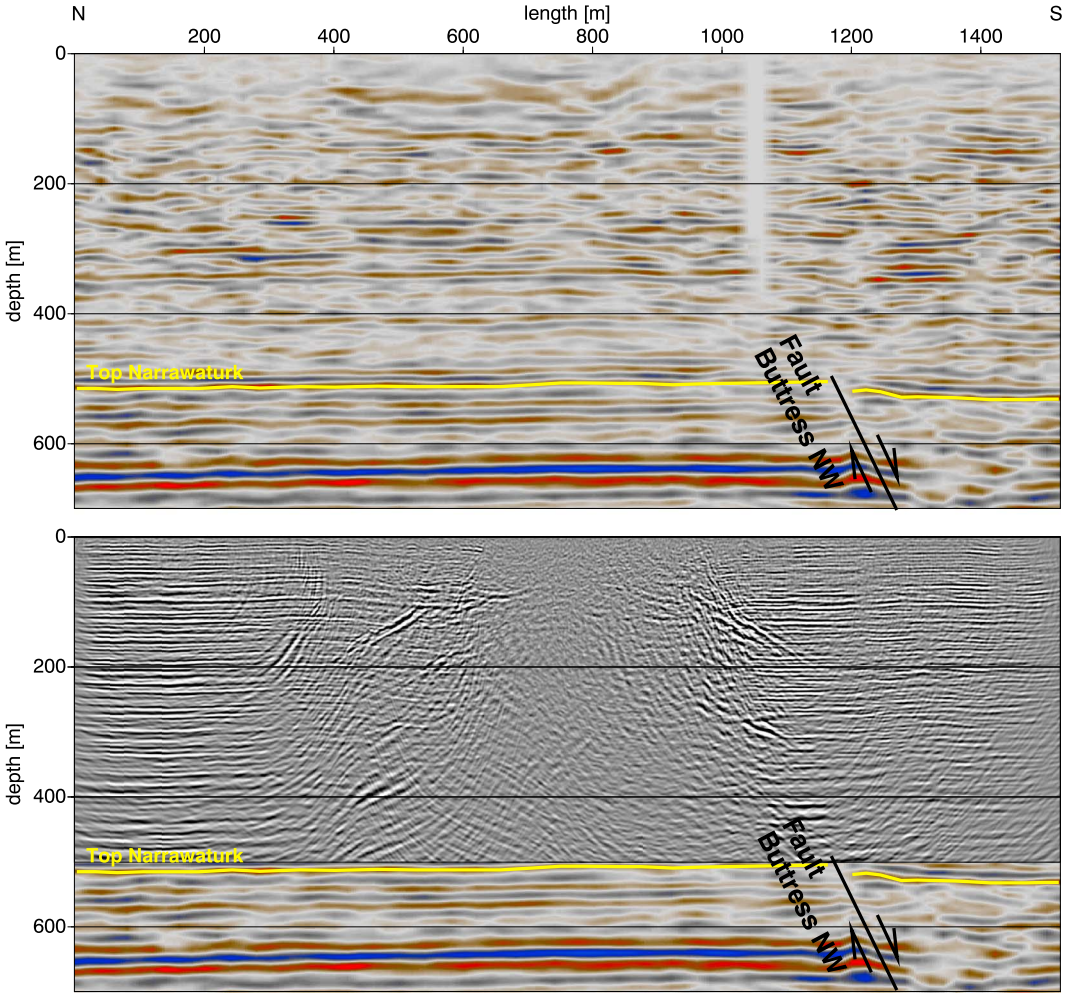

Figure 13. Cross sections along profile PROTECT 2. (top) *P* wave section from seismic cube Nirranda-Heytesbury 3-D at sea level datum with interpretation [*Ziesch et al.*, 2015]. (bottom) Shear wave cross section overlain.

5.2. Profile PROTECT 2

Profile PROTECT 2 is ~1470 m long and is the longest of the three profiles discussed here. The interpretation of the regional 3-D *P* wave data indicates that Buttress NW Fault, if extrapolated upward by dip, would reach the surface in the southern third of the profile (Figures 3 and 13, top). Similar to PROTECT 1, the normal fault cannot be interpreted above ~500 m below sea level, which is approximately the top of Narrawaturk Formation. Instead, some continuous horizontal reflectors are present between 100 and 400 m depth (Figure 13, top), albeit with subordinate interruptions. In any case, the reflections are more continuous than in the *P* wave data along PROTECT 1 (cf. Figure 11).

The newly acquired shear wave section along PROTECT 2 is overlain on top of the uppermost 500 m of the *P* wave profile (Figure 13, bottom). The difference between the *P* wave and the shear wave sections is surprisingly large. The center part of the shear wave profile is strongly disturbed, whereas the *P* wave section presents comparably undisturbed reflectors in the same region of the section (Figure 13 bottom, between 600 and 1000 m profile length).

The detailed interpretation of the shear wave cross section suggests that the southern limit of this diffuse zone can be described by the extrapolation of the normal fault imaged at 500 m depth in the *P* wave data (Figure 14, bottom). Maintaining its dip of ~60°, the fault can be imaged in the shear wave data all the way to the surface (sea level datum). Especially between 0 and 300 m depth, a distinct shear wave reflection is observed (Figures 13, bottom, and 14, bottom, solid red line). Some related synthetic and antithetic faults can also be interpreted (Figure 14, bottom, dashed red lines).

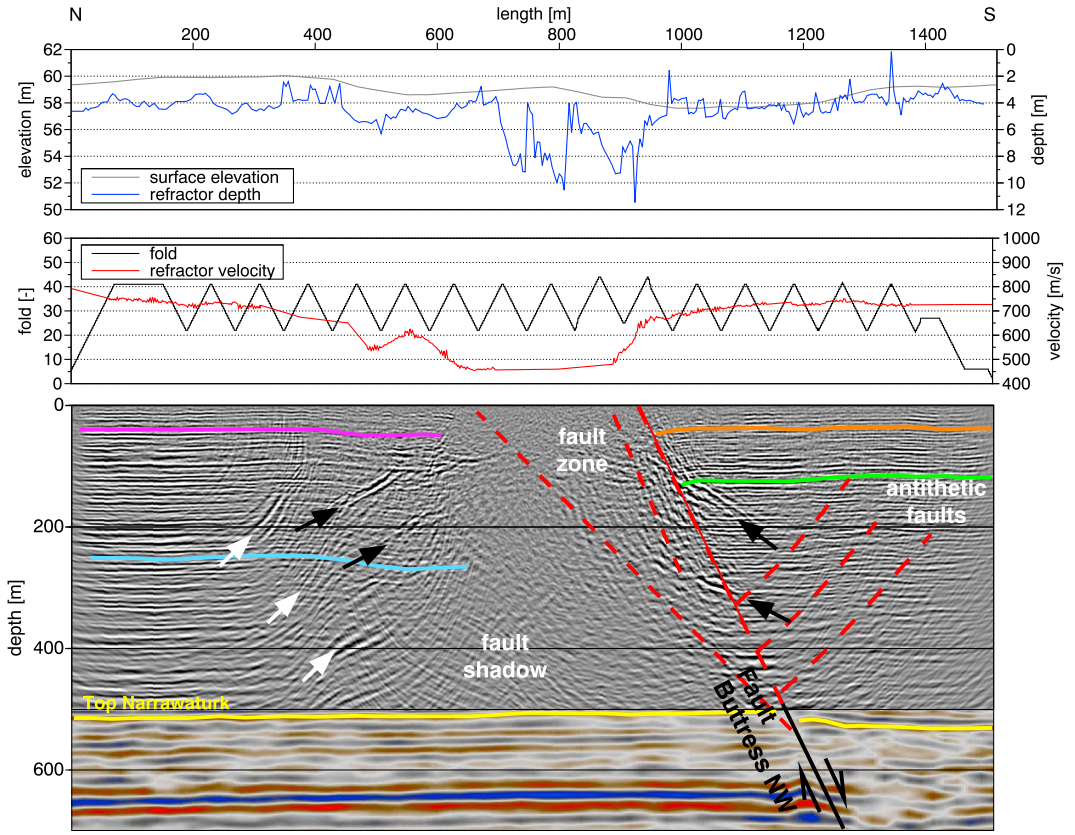

Figure 14. Detailed structure of PROTECT 2. (top) Surface elevation and refractor properties from the shear wave data. (bottom) Interpretation of the high-resolution shear wave image at sea level datum. Black arrows indicate misplaced straight onsets, white arrows indicate migration smile-like onsets that seem to be misplaced not only because of an insufficient velocity model.

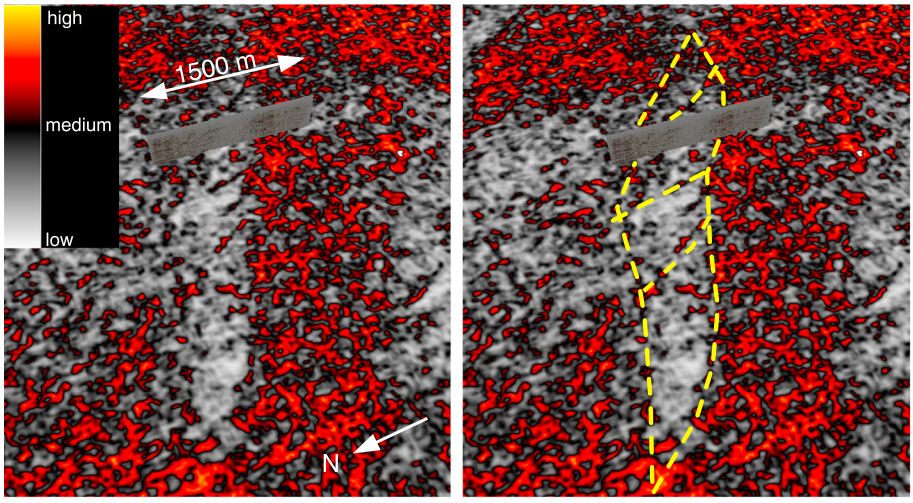

Figure 15. Perspective view of a combination of the shear wave profile PROTECT 2 and a depth slice at 432 m bsl of the variance cube calculated from the Nirranda-Heytesbury 3-D *P* wave survey. The yellow lines indicate extent and internal segmentation of the presumed fault zone, exhibited by increased transparency.

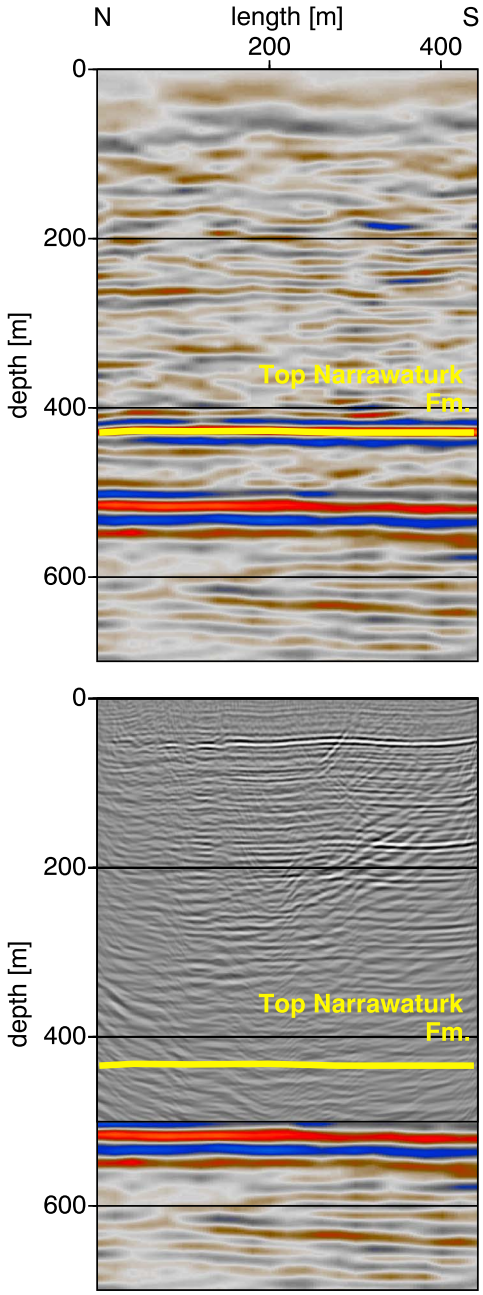

Figure 16. Cross sections along profile PROTECT 3. (top) *P* wave section from seismic cube Nirranda-Heytesbury 3-D at sea level datum with interpretation [*Ziesch et al.*, 2015]. No obvious fault zones can be identified. (bottom) Shear wave cross section overlain.

The central part of the *S* wave profile shows far less structural detail than the northern and southern ends, due to reduced amplitudes and bandwidth of the signals. This blurry image is caused by the reflections of the fault zone branches that apparently reduce the reflected signal energy from below, thereby causing a fault shadow in the section (Figure 14, bottom, 700–900 m profile length). Along PROTECT 2 this effect is much stronger than along PROTECT 1 (cf. Figure 12, bottom).

Along PROTECT 2 additional strong evidence of near-surface faulting exists. The topography, shear wave refractor depth, and refractor velocity all show considerable variation along the profile, and the strongest refractor anomalies correlate with those parts of the shear wave profile that are the most disturbed (Figure 14 top, between 600 and 1000 m profile length).

It is clear that additional structural features must exist in the section, not all of which can be easily interpreted as part of the faulting process. Some of them are probably related to the 3-D nature of the subsurface. Since the shear wave survey had a 2-D geometry, it can be expected that some structural features in the image were misplaced during the 2-D imaging procedure. This is evident for the straight onsets indicated with black arrows. However, this also seems to be true for some of the migration smile-like onsets, especially north of the central part of the section, marked with white arrows. The migration velocity seems to be only partly responsible for their shape. In any case, a lot of detail can be identified in the section that strongly supports the interpretation of the upward continuation of Fault Buttress NW.

We merged the shear wave profile PROTECT 2 with a depth slice at 432 m bsl of the variance cube calculated from the Nirranda-Heytesbury 3-D survey, in order to find evidence of faults or fractures in the 3-D data. Such variance calculations are a standard means for such analysis in seismic data sets, especially in time or depth slices [e.g., *Chopra and Marfurt*, 2007]. The most striking observation is that the center part of the 2-D profile is located in an area of the 3-D *P* wave data that shows very low variance, compared with the neighboring sections (Figure 15). This coincides with the observation of a seemingly less disturbed center part in the *P* wave cross section (Figure 14, top). However, inside this less disturbed section a number of splay faults can be identified (Figure 15, marked in yellow). Reflections off such faults in the 2-D shear wave section would be misplaced during seismic data processing. The observation of splay faults suggests a strike-slip component in this fault zone.

From the above observations it can be concluded that, in fact, Fault Buttress NW does reach all the way from depth to the surface. Shear waves are attenuated because the fault zone is intensely structured and the

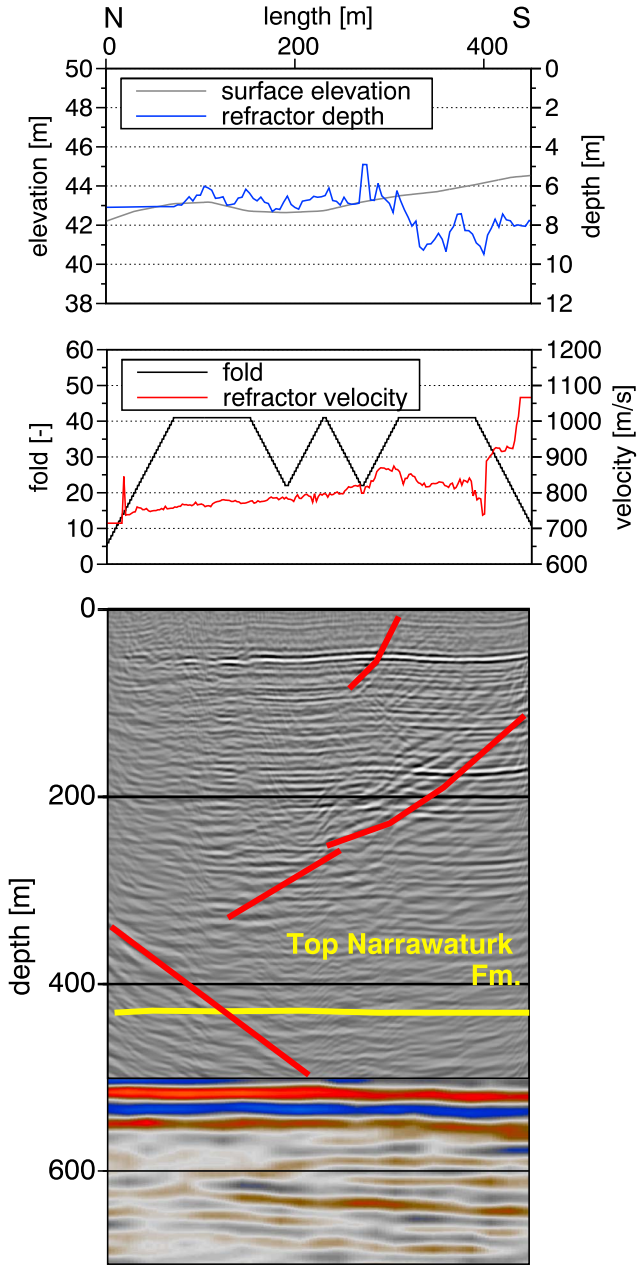

Figure 17. Detailed structure of PROTECT 3. (top) Surface elevation and refractor properties from the shear wave data. (bottom) Interpretation of the high-resolution shear wave image at sea level datum.

near-surface horizons are deteriorated accordingly. This deterioration is stronger than at PROTECT 1 because the fault throw of the underlying sequences is obviously larger (cf. Figures 2 and 3). The normal fault nature of Buttress NW also results in a more pronounced shadow effect, in contrast to the inversion structure interpreted in PROTECT 1.

5.3. Profile PROTECT 3

To image the integrity of the overburden with high resolution, profile PROTECT 3 was shot close to the CRC wells. The *P* wave cross section of the 3-D data set (Figure 16, top) does not show any interpretable features above the top of Narrawaturk Formation, except some vague horizontal events. However, if the shear wave section is taken into account (Figures 16 and 17, bottom), it becomes clear that three distinct fault traces at different depths and in different parts of the section are clearly imaged as fault planes. At largest depth, a fault trace can be observed that reaches from Top Mepunga in the center of the profile up to ~350 m bsl at

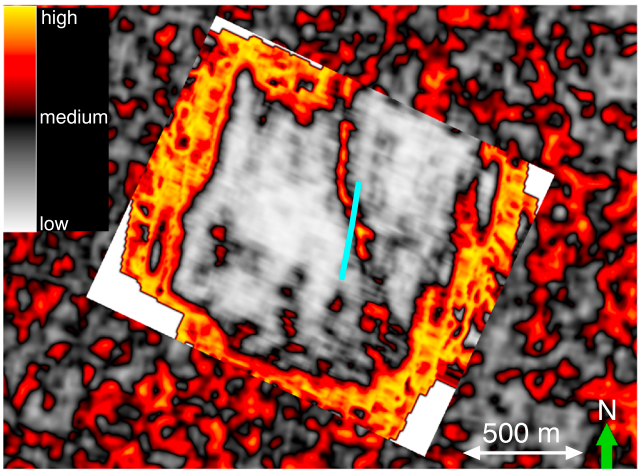

Figure 18. Overlay of two depth slices at 321 m bsl of the variance cubes calculated from the Nirranda-Heytesbury and the Otway 3D surveys. The location of the shear wave profile PROTECT 3 is indicated in blue.

its northern end (Figure 17, bottom, 0–200 m profile length). If this fault structure indication is extrapolated to the surface, it would outcrop at a small topographic low, accordingly observed in the field to the north of the profile.

At intermediate section depth, another fault zone reaches from ~350 m bsl to ~100 m bsl (Figure 17, bottom, 150–420 m profile length). Instead of a single reflection, a number of onsets can be identified. None of these seems to offset any of the horizons. Therefore, some 3-D effect, i.e., sideswipe signals, may be present.

To analyze this in more detail, we studied variance calculations of two *P* wave data sets: the seismic cube Nirranda-Heytesbury 3-D at sea level datum [*CGG Australia Pty. Ltd.*, 2000] and the small survey Otway 3D that was acquired at the CO2CRC Otway Project site [*Pevzner et al.*, 2010]. These variance cubes are cut at 321 m bsl, which is the lower end of the fault trace imaged in the shear wave profile. The overlay clearly shows that a variance anomaly occurs at this depth level (Figure 18; blue line marks location of PROTECT 3) with high values met in the northern half of the shear wave profile. Since the variance slice of the Otway 3D data reaches its fold limit at this depth, the values at its boundaries' edges are noisy.

The observed N-S trending variance anomaly at the center of the depth slice can be interpreted as a fault that strikes at an acute angle to the shear wave profile. This fault can be regarded as the source of misplaced, dipping reflectors in Figures 16 and 17. However, if the fault trace interpreted in the shear wave seismic section is extrapolated to the surface, it would end at a small hill, the top of which reaches ~50 m elevation asl to the south of the profile.

In the upper half of the shear wave section there are indications of additional fault zones or fractures (Figure 17, bottom, at ~300 m profile length). The outcrop of the interpreted short fault zone above 100 m bsl, close to the center of the profile, is located where the refractor depth drops from ~7 m in the northern part of the profile to ~9 m in the southern part (Figure 17, top). Such depth difference between the units north and south of this small fracture are not identified in the reflectors in the shear wave profile, even though we would expect a 2 m shift to be barely imageable with the shear waves.

6. Discussion

One of the aims of the 2-D near-surface shear wave reflection measurements at the CO2CRC Otway Project site was to determine the near-surface characteristics of deeper faults in the near subsurface. If they would all terminate at a certain depth level, such termination could be regarded as an additional safety barrier in case of CO_2 leakage from the storage formation at depth. If faults do extend to the surface, they may provide a potential migration pathway to the surface. Although none of the major faults in the direct vicinity of the Naylor structure are interpreted in the existing *P* wave data to reach the surface, fault zones in the proximity that pass through the top reservoir horizon may have an impact on a possible long-term migration scenario. Near-surface sections above the fault zones Buttress NW and Fault 2 were therefore targeted for shear wave profiles.

Along profiles PROTECT 1 and 2, the newly acquired 2-D shear wave images indeed suggest a continuation of the deeply reaching fault zones to the surface (Figures 12 and 14). This is not the case at profile PROTECT 3, where the fault zone Naylor South dies out at ~800 m bsl in the interpreted 3-D *P* wave data [*Ziesch et al.*, 2015]. Even though the new shear wave seismic image of the structures above this fault zone also shows indications of near-surface faults, no direct continuation of the deep structures can be made with faults at the surface (Figure 17).

6.1. Combination of Surface and Seismic Subsurface Data

Near-surface expressions of fault activity exist along the coast in the proximity of the Otway project site. Such structures are prominently found at Twelve Apostles, on the south coast of Australia, near Port Campbell, Victoria. The cliff exhibits three different fault types (labeled I–III in Figure 19): a thrust (reverse) fault with a throw of ~2 m is located next to a strike-slip fault, which in turn is located beside a normal fault system. It is evident that near-surface structures in this region can be complex in detail.

Imaging of subtle near-surface structures is the strength of high-resolution shear wave reflection seismic surveying, which has been increasingly successful during recent years [e.g., *Inazaki*, 2004; *Polom et al.*, 2010, 2013; *Pugin et al.*, 2013; *Krawczyk et al.*, 2013; *Ghose et al.*, 2013]. In the Otway area, compressional inversion is evident with throws of only 2 m near the surface, as indicated in outcrop (Figure 19) or interpreted from refractor steps in seismic data (Figure 17, top). However, as 2 m is close to the resolution limit of our shear wave measurements, source frequencies of up to ~240 Hz should be utilized at this site in future surveys, to ensure more detailed structural imaging and analysis of such a throw in the nearest subsurface, with the side effect of compromising shear wave depth penetration.

Detailed topographic information could generally act as additional deformation proxy, for instance, used in Western Australia or the Basin and Range province [*Whitney and Hengesh*, 2015; *Hilley et al.*, 2001] or reviewed in [*Davies et al.*, 2007], as well as for seismic site conditions [e.g., *Wald and Allen*, 2007]. In the investigation area, topographic variation is too sparse to reflect subtle fault strike signals of seemingly ~2 m in the region. The larger-scale elevation variation at the northern end of profile PROTECT 1, close to the Curdie River, however, would seem to be large enough to be represented by the local topographic data. Here it correlates with our interpretation of an inversion-related structure (Figure 12). Along with the seismic survey we recorded Differential Global Positioning System (DGPS) positions of station coordinates and were thus able to correlate small-scale structure variations with the topography.

While the topographic information of our survey also corroborates the seismic structure of profile PROTECT 2, the elevation profile in the vicinity of the CRC boreholes (profile PROTECT 3) does not show any anomalies that can be related to faults or fractures in the subsurface. This may be related to the fact that the faults reach the surface off the profile or are in fact out of plane of the seismic section. A topographic high ~100 m south of the southern profile end is formed by a known dune structure [*Schacht et al.*, 2011; *Edwards et al.*, 1996]. Therefore, the strike directions of the surface feature and the subsurface faults (Figures 17 and 18) do not correspond. A high-resolution digital elevation model of the region would perhaps be able to delineate such structures at surface.

Surface expressions of fault zones may not always be traced by clear fault plane images in the uppermost levels of a final seismic cross section, because prestack processing, migration and stacking procedures, or simply the resolution of the signals often hamper the proper imaging of the nearest-surface anomalies. In our case study, we had to remove geophone traces that were closer than 20 m of the shot point, because of filter noise related to strong surface wave interference. Thus, the associated absence of earliest reflection arrivals hampered the imaging of the very uppermost units. An additional identification of features in the original shot records can thus be an important aid to interpret near-surface extrapolations of deeper structures and can clarify the geological situation.

6.2. Fault Indicators in Shot Data

Typical shot records along profiles PROTECT 1 and 2 show such first-order anomalies as individual first-break signatures. Along PROTECT 1, the different shot records show distinct onsets of the first breaks, except for the northernmost end of the profile (Figures 5a, 5b, 7a, and 7b), where first-break onsets show a more complicated signature. The first break between 0 and 40 m length shows very low apparent velocities (Figures 5b and 7b), as at the northern end of the profile (Figures 5a and 7a), where not just some of the geophone locations, but also the shot location lie within this low-velocity section, so that the whole record lacks a distinct

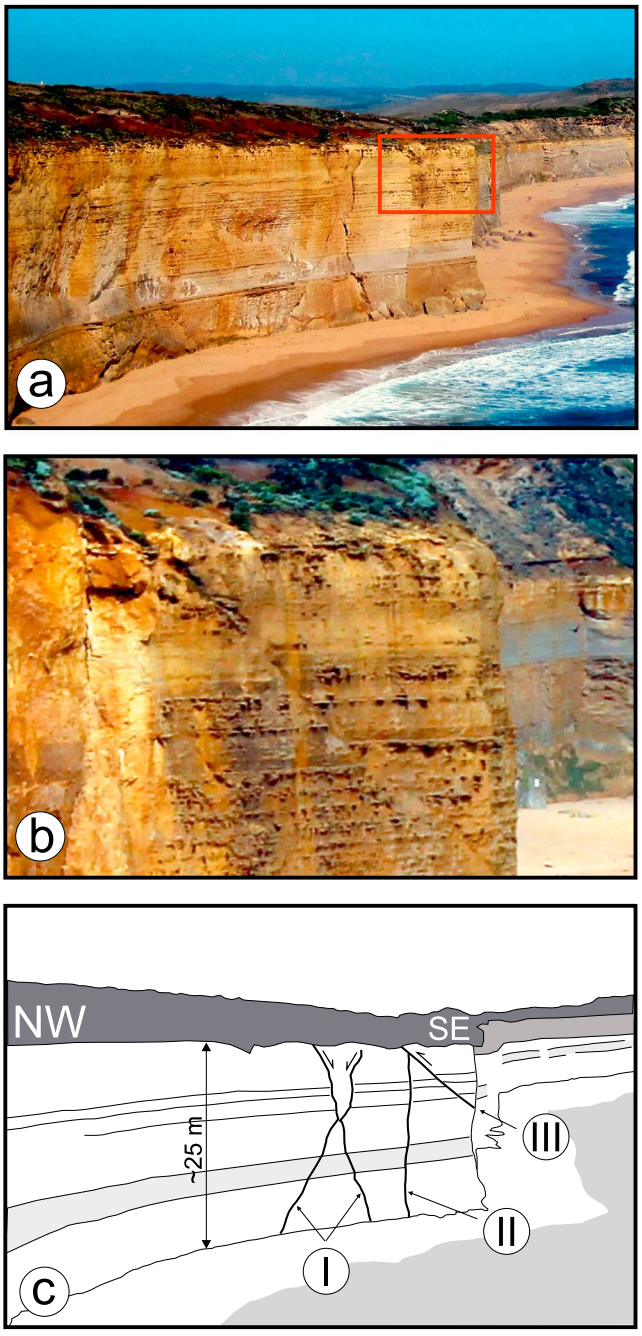

Figure 19. Cliff at Twelve Apostles, south coast of Australia near Port Campbell, Victoria (30°40′02.17″S, 143°06′28.83″E). (a) View looking east (November 2012) with red frame indicating (b) the area shown as detailed view (November 2013). (c) The interpretation shows three fault types: (I) conjugate normal fault, (II) strike-slip fault with unknown shear sense, and (III) thrust fault.

first break. The first-break interpretation thus identifies a location 40 m south of the northern end of the profile as the location carrying the surface expression of the top of the hanging wall of deeply reaching Fault 2 (c.f., Figure 12).

First-break signatures in shot records along profile PROTECT 2 (Figures 6 and 8) show stronger indications of near-surface fault expressions influenced by the deeply reaching fault zone—in this case Buttress NW. Shot records at the northern and southern ends of the profile (Figures 6a, 6f, 8a, and 8f) show high-bandwidth reflections and distinct first-break signals, similar to most of PROTECT 1. The closer the shot record to the

center of the profile, the less bandwidth, the slower the direct waves (white arrows), and the less distinct the first-break signature. This correlates with the observation that the center of the profile between 600 and 900 m length are influenced by fault Buttress NW (c.f., Figure 14).

Sometimes, the coincidence of a fault zone with the incident direct or refracted wave, i.e., first break, results in a reflected direct or refracted wave. If the strike of such a fault zone is perpendicular to the seismic profile, the apparent velocities of incident and reflected waves are equal. At the northern end of PROTECT 1 the loss of first-break distinction, for example, correlates with a reflection of the first-break onset signal (red arrows in Figure 5). This could be interpreted as a reflected refraction. This would mean that the signal that is interpreted as a reflection off a fault plane is, in fact, a refracted wave. However, the apparent velocity of the incident wave is ~790 m/s, whereas the apparent velocity of the corresponding reflected waves is ~1200 m/s. If these reflected onsets represent refractions, this would require an angle between profile and fault strike of ~53° to reach this apparent velocity. This is much higher than we expected prior to the measurements, when we assumed a ~20° azimuth difference (Figure 1).

More complex models to explain the reflection as a direct or refracted wave involve either shear wave to *P* wave mode conversion or the excitation of *P* waves oblique to the seismic profile by the seismic source. The latter case is not unusual and is described by, e.g., *Pugin et al.* [2004]. However, as we do not have any 3-D structure control near the surface close to the PROTECT 1 profile, this aspect remains speculative. A way to circumvent this 3-D challenge in future surveys could be the use of seismic three-component receivers [e.g., *Malehmir et al.*, 2015]. However, depending on wave interference, polarization analysis can be misleading or inaccurate. Therefore, the additional use of a narrow 3-D survey, either by using parallel spreads of receivers (one road width) or the frequent use of crossline shot points (one road width), could help solve this spatial ambiquity, by making use of crossline slowness.

Since we identified some minor horizon throw on the interpreted reverse fault and steps in the interpreted fault reflections (Figure 12), we suggest that these onsets are in fact shear wave reflections off the reverse fault surface and not just reflected refractions. In summary, the shot records support the interpretation of near-surface extensions of deeply reaching fault zones in the region.

6.3. Influence of Survey Setup and Surface Properties

Apart from the geometrical prerequisite to measure perpendicular to the strike of fault zones, we had planned to measure on paved roads as much as possible, since road pavement often suppresses surface waves such as Love waves [e.g., *Inazaki*, 2004; *Hoffmann et al.*, 2008; *Krawczyk et al.*, 2013]. However, for practical reasons, profile PROTECT 2 had to be carried out on the compacted gravel surface of Baileys Road and profile PROTECT 3, in the direct vicinity of the CRC boreholes, had to be measured along Sodas Lane, which is a gravel road as well. Only profile PROTECT 1 could be facilitated on the asphalt surface of Whiskey Creek Road.

We did not try to suppress surface waves (Love waves) by using a fixed geophone pattern in the data acquisition process [e.g., *Milkereit et al.*, 1986], since we did not want to suppress any possible reflections off faults or fractures. This corresponds to the experience of *Bexfield et al.* [2006], who surveyed the New Madrid seismic zone, Mississippi, to investigate the relationship between deep and shallow deformational features in the area. Instead, we carefully removed the surface wave onsets successfully with fk filtering after data acquisition, leaving dipping onsets in the shot records (Figures 5–8).

A methodological aspect regarding the shot records is the existence of surface waves along profile PROTECT 1. Surprisingly, all shots show surface waves (black arrows, Figure 5), even though this profile had been acquired with sources and geophones on a paved asphalt road. Experience has shown that road pavement is able to suppress the buildup of surface waves (Love waves) during *SH* wave reflection measurements, an observation that has been explained with a high seismic velocity surface layer, i.e., an inverted velocity-depth profile at the surface [e.g., *Inazaki*, 2004; *Pugin et al.*, 2004; *Hoffmann et al.*, 2008; *Krawczyk et al.*, 2013]. This is often regarded as a key aspect when acquiring high-quality *SH* waves, especially in urban environments. Apparently in this case, the asphalt shear wave velocities are below the velocities of the lower units, which can be related to the pavement composition or surface temperature. Therefore, it must be concluded that road pavement does not suppress Love wave buildup under all circumstances.

An important observation is the strong reflection amplitudes of many of the interpreted fault zones, even up to the point of the existence of a fault shadow. More than the *P* wave transmission, shear wave transmission is dependent on rock matrix integrity, because in the latter case it is a function of the shear modulus only.

If faults and fault damage zones cover a large area, a shear wave is more strongly reflected than a *P* wave, because *P* waves are also transmitted through fluids in the porous portion of fractures [*Burschil and Krawczyk*, 2016]. Other signal attenuation mechanisms can be scattering and wave conversion, which needs some 3-D fracture orientation for strong attenuation, if *SH* waves are used as source signals. Current shear wave finite-difference modeling algorithms typically do not account for this effect at rock unit interfaces, for instance, if some modeling approach is to be utilized to better comprehend the nature of the reflections found in the data [e.g., *Burschil et al.*, 2015].

Fault shadows may also be introduced by incomplete or destructive signal stacking. In this case, not only the velocity model of the subsurface but also the migration method plays an important role. If lateral velocity variations exist, which can be expected in the context of fault zones, depth migration is the preferred migration method. If conflicting dips are present as well, prestack depth migration should be used. So far, we have only applied prestack time migration. Therefore, it can be expected that imaging improvement would be possible with prestack depth migration.

The shear wave velocities we have determined so far would serve as good starting models for depth migration, even though we do not have good independent control in the near surface. Sonic log shear wave velocities from borehole CRC-2 [*Dance*, 2010] are unreliable above ~650 m depth, even though the used tool provides six different sensor configurations. In this part of the borehole the velocities are below the velocity of the compressional wave in water, a common problem of sonic log shear wave velocity determination. Shear wave analyses reported by *Pevzner et al.* [2011] from a Vertical Seismic Profile (VSP) that had been carried out in the CRC-1 borehole (cf. Figure 1) are only shown below 500 m depth. The Vp-to-Vs relationship at the shown depth levels is of the order of 2.

During the processing procedure, fk filtering proved positive. This corresponds to *Pugin et al.* [2004], who report that they usually do not apply fk filtering on data collected on unconsolidated (slow) ground, so as not to suppress dipping events, yet to use a fk filter with data collected on harder ground. We have not yet tried median filtering that is sometimes successfully applied in VSP data processing as an alternative approach. Another beneficial process was the application of refraction statics. This is in contrast to our previous experience [e.g., *Krawczyk et al.*, 2013] and others' experience [e.g., *Pugin et al.*, 2013; *Bexfield et al.*, 2006]. On the other hand, *McBride et al.* [2010] state that they applied static corrections successfully, although it is not clear whether they refer to their *P* wave or *SH* wave surveys singularly or together.

Speculation about sideswipe effects, i.e., whether they are reflections or refractions, could to some degree be tackled using a modeling approach. This would have to be 3-D and may therefore be restricted to ray-tracing techniques instead of finite-difference modeling of the complete wave field.

7. Conclusions

All three shear wave profiles cross fault zones with near-surface expression. Whereas PROTECT 1 and 2 show a near-surface connection to the deeply reaching fault zones Fault 2 and Buttress NW, respectively, PROTECT 3 exhibits small-scale structures at different depths. Especially PROTECT 2 shows that the rock integrity is disturbed within the fault zones, which causes strong shear wave attenuation and thus fault shadow, i.e., the signals are not able to travel across certain parts of the fault zone because the rock matrix is disturbed.

Since the profiles were acquired across fault zones, lateral velocity contrasts are likely to exist that we were not able to determine with a standard Normal Moveout (NMO)/DMO velocity model. Therefore, we suggest that further insight into the structures could be gained by applying prestack depth migration with reflection tomography and ray-tracing velocity update.

Concerning CO_2 storage safety, it should be noted that even though the individual fault geometries along the profiles differ, the faults have to be considered as comprehensive zones of faults and fractures. Here the measured shear wave velocities can allow enhanced rock parameter analysis.

We propose that it is feasible to complement large-scale seismic exploration surveying with high-resolution shear wave measurements. Indeed, we also propose dedicated small-scale high-resolution near-surface 3-D *P* wave surveys in the areas of question, since they are less influenced by rock matrix alterations. Thereby, a better probing of seal integrity and the evaluation of the existence of possible pathways in the near surface is enabled, which can lead to a better defined monitoring strategy for an area.

Acknowledgments
We gratefully acknowledge support by Josie McInerney, Matthias Raab, Rajindar Singh, and Peter Dumesny of CO2CRC; Tess Dance, Roman Pevzner, Anton Kepic, Milovan Urosevic, and Boris Gurevich of Curtin University; and Sven Wedig of LIAG. We also thank four anonymous reviewers for their valuable input that helped improve this article. This work was sponsored in part by the Australian Commonwealth Government through the Cooperative Research Centre for Greenhouse Gas Technologies (CO2CRC). PROTECT was funded through the GEOTECHNOLOGIEN research program in Germany (grant 03G0797). The data used are listed in the references and tables. The seismic profiles and interpretations are available from the first author upon request.

References

Al-Jabri, Y., and M. Urosevic (2010), Assessing the repeatability of reflection seismic data in the presence of complex near-surface conditions, CO2CRC Otway Project, Victoria, Australia, *Explor. Geophys.*, *41*(1), 24–30, doi:10.1071/EG09010.

Beilecke, T., C. Krawczyk, D. Tanner, J. Ziesch, and PROTECT Research Group (2014a), Poisson's ratio model derived from *P*- and *S*-wave reflection seismic data at the CO2CRC Otway Project pilot site, Australia, paper presented at 26th EGS General Assembly, vol. 16, Vienna, Austria, 27 April to 2 May.

Beilecke, T., C. Krawczyk, and D. Tanner (2014b), Seismic Program closeout report—Shallow shear wave data acquisition survey, *Tech. Rep. CO2CRC Publ. Number RPT14-4950*, Coop. Res. Cent. for Greenhouse Gas Technol., Canberra, Australia.

Bexfield, C., et al. (2006), Integration of *P*- and *SH*-wave high-resolution seismic reflection and micro-gravity techniques to improve interpretation of shallow subsurface structure: New Madrid Seismic Zone, *Techtonophysics*, *420*(1–2), 5–21, doi:10.1016/j.tecto.2006.01.024.

Burschil, T., T. Beilecke, and C. Krawczyk (2015), Finite difference modelling to evaluate seismic *P*-wave and shear wave field data, *Solid Earth*, *6*(1), 33–47, doi:10.5194/sed-6-33-2015.

Burschil, T., and C. Krawczyk (2016), Modelling study of challenges in sinkhole detection with shear wave reflection seismics, paper presented at 28th EGS General Assembly, vol. 18, Vienna Austria, 17–22 Apr.

CGG Australia Pty. Ltd. (2000), Curdie vale 3D seismic data processing, *Final Report, Tech. Rep.*, CGG Australia Pty., West Perth, Western Australia.

Chopra, S., and K. Marfurt (2007), *Seismic Attributes for Prospect Identification and Reservoir Characterization, Geophys. Dev. Ser.*, Soc. of Explor. Geophys., Calgary, Alberta.

Cook, P. (Ed.) (2014), *Geologically Storing Carbon: Learning From the Otway Project Experience*, CSIRO, 408 pp., Melbourne, Victoria, Australia.

Dance, T. (2010), Core and well log analysis from the CRC-2 well: CO2CRC Otway Project phase II, *Tech. Rep. CO2CRC Publ. Number RPT10-2221*, Coop. Res. Cent. for Greenhouse Gas Technol., Canberra, Australia.

Davies, R., H. Posamentier, L. Wood, and J. Cartwright (Eds.) (2007), *Seismic Geomorphology: Applications to Hydrocarbon Exploration and Production*, vol. 277, 288 pp., Geol. Soc. Spec. Publ., London.

Deregowski, S. (1986), What is DMO?, *First Break*, *4*(7), 7–24.

Dix, C. (1955), Seismic velocities from surface measurements, *Geophysics*, *20*, 68–86.

Edwards, J., S. Tickell, C. Abele, A. Willocks, A. Eaton, R. King, and S. Bourton (1994), Port Campbell Embayment 1:100000 geological map, *Tech. Rep.*, Geol. Surv. of Victoria, Melbourne, Australia.

Edwards, J., S. Tickell, A. Willocks, A. Eaton, M. Cramer, R. King, and S. Bourton (1996), Colac 1:250000 geological map, *Tech. Rep. 98*, Geolog. Surv. of Victoria, Melbourne, Australia.

Geoscience Australia (2015), Australian stratigraphic units database. [Available at http://dbforms.ga.gov.au/www/ geodx.strat_units.int], online; accessed: 30-March-2015.

Ghose, R., J. Carvalho, and A. Loureiro (2013), Signature of fault zone deformation in near-surface soil visible in shear wave seismic reflections, *Geophys. Res. Lett.*, *40*, 1074–1078, doi:10.1002/grl.50241,2013.

Gulunay, N. (1985), A new method for the surface-consistent decomposition of statics using diminishing residual matrices (DRM), SEG Technical Program Expanded Abstracts, presented at 55th SEG Annual Meeting, pp. 293–295, Society of Exploration Geophysicists.

Hilley, G., J. Arrowsmith, and L. Amoroso (2001), Interaction between normal faults and fractures and fault scarp morphology, *Geophys. Res. Lett.*, *28*(19), 3777–3780.

Hoffmann, S., T. Beilecke, U. Polom, U. Werban, C. Leven, and B. Engeser (2008), Integrierter Einsatz von Scherwellenseismik und Direct-Push-Verfahren zur Erkundung eines urbanen Grundwasserleiters, *Grundwasser*, *13*(2), 78–90, doi:10.1007/s00767-008-0067-8.

Holford, S. P., A. K. Tuitt, R. R. Hillis, P. F. Green, M. S. Stoker, I. R. Duddy, M. Sandiford, and D. R. Tassone (2014), Cenozoic deformation in the Otway Basin, Southern Australian margin: Implications for the origin and nature of post-breakup compression at rifted margins, *Basin Res.*, *26*, 10–37, doi:10.1111/bre.12035.

Hollingshead, G., and R. R. Slater (1979), A novel method of deriving weathering statics from first arrival refractions, Abstracts presented at 49th Annual Meeting and Exposition, Society of Exploration Geophysicists.

Hortle, A., P. de Caritat, C. Stalvies, and C. Jenkins (2011), Groundwater monitoring at the Otway Project site, Australia, *Energy Procedia*, *4*, 5495–5503, doi:10.1016/j.egypro.2011.02.535.

Inazaki, T. (2004), High-resolution seismic reflection surveying at paved areas using an *S*-wave type land streamer, *Explor. Geophys.*, *35*(1), 1–6, doi:10.1190/tle32010032.1.

Jenkins, C. R., et al. (2011), Safe storage and effective monitoring of CO_2 in depleted gas fields, *Proc. Natl. Acad. Sci. U.S.A.*, *109*(2), E35–E41.

Kallweit, R., and L. Wood (1982), The limits of resolution of zero-phase wavelets, *Geophysics*, *47*(7), 1035–1046.

Krawczyk, C., D. Tanner, A. Henk, H. Tappe, and M. Urosevic (2011), Sub-/seismic deformation prediction—Development of a new seismo-mechanical workflow in the Otway Basin,paper presented at 1st Sustainable Earth Sciences Conference and Exhibition, pp. 208–212, doi:10.3997/2214-4609.20144172.

Krawczyk, C., U. Polom, and T. Beilecke (2013), Shear-wave reflection seismics as a valuable tool for urban applications, *Leading Edge*, *32*(3), 256–263, doi:10.1190/tle32030256.1.

Krawczyk, C., et al. (2015), Seismic and sub-seismic deformation prediction in the context of geological carbon trapping and storage, in *Geological Storage of CO_2—Long Term Security Aspects, Advanced Technologies in Earth Sciences, Geotechnologien Sci. Rep. No. 22*, edited by A. Liebscher and U. Münch, pp. 97–113, Springer, Berlin.

Lawton, D. (1989), Computation of refraction static corrections using first-break traveltime differences, *Geophysics*, *54*, 1289–1296.

Malehmir, A., M. Bastani, C. Krawczyk, M. Gurk, N. Ismail, U. Polom, and L. Persson (2013), Geophysical assessment and geotechnical investigation of quick-clay landslides—A Swedish case study, *Near Surf. Geophys.*, *11*, 341–350, doi:10.3997/1873-0604.2013010.

Malehmir, A., S. Wang, J. Lamminen, B. Brodic, M. Bastani, K. Vaittinen, C. Juhlin, and J. Place (2015), Delineating structures controlling sandstone-hosted base-metal deposits using high-resolution multicomponent seismic and radio-magnetotelluric methods: A case study from northern Sweden, *Geophys. Prospect.*, *63*, 774–797, doi:10.1111/1365-2478.12238.

McBride, J., W. Stephenson, R. Williams, J. Odum, D. Worley, J. South, A. Brinkerhoff, R. Keach, and A. Okojie-Ayoro (2010), Shallow subsurface structure of the Wasatch Fault, Provo segment, Utah, from integrated compressional and shear-wave seismic reflection profiles with implications for fault structure and development, *Bull. Geol. Soc.*, *122*(11–12), 1800–1814, doi:10.1130/B30174.1.

Milkereit, B., H. Stümpel, and W. Rabbel (1986), Shear-wave reflection profiling for near-surface lignite exploration, *Geophys. Prospect.*, *34*, 845–855.

Norvick, M., and M. A. Smith (2001), Mapping the plate tectonic reconstructions of southern and southeastern Australia and implications for petroleum system, *APPEA J.*, *41*, 15–35.

Palmer, D. (1980), The generalized reciprocal method of seismic refraction interpretation, *Soc. of Explor. Geophys., Tulsa, USA*, doi:10.1190/1.9781560802426.
Palmer, D. (1986), *Refraction Seismics, Handbook of Geophys. Explor. Ser.*, vol. 13, edited by K. Helbig and S. Treitel, Geophys. Press, London.
Perincek, D., and C. Cockshell (1995), The Otway Basin: Early Cretaceous rifting to Neogene inversion, *Aust. Pet. Explor. Assoc. J.*, *35*, 451–466.
Pevzner, R., V. Shulakova, A. Kepic, and M. Urosevic (2010), Repeatability analysis of land time-lapse seismic data: CO2CRC Otway Pilot Project case study, *Geophys. Prospect.*, *59*(1), 66–77, doi:10.1111/j.1365-2478.2010.00907.x.
Pevzner, R., B. Gurevich, and M. Urosevic (2011), Estimation of azimuthal anisotropy from VSP data using *S*-wave velocity analysis, *Geophysics*, *76*(5), D1–D9, doi:10.1190/GEO2010-0290.1.
Polom, U., L. Hansen, G. Sauvin, J.-S. L'Heureux, I. Lecomte, C. Krawczyk, M. Vanneste, and O. Longva (2010), High-resolution *SH*-wave seismic reflection for characterization of on-shore ground conditions in the Trondheim harbour, central Norway, in *Advances in Near-Surface Seismology and Ground-Penetrating Radar*, edited by R. Miller, J. Bradford, and K. Holliger, pp. 297–312, Soc. of Explor. Geophys., Tulsa, USA.
Polom, U., M. Bagge, S. Wadas, J. Winsemann, C. Brandes, F. Binot, and C. Krawczyk (2013), Surveying near-surface depocentres by means of of shear wave seismics, *First Break*, *31*(8), 67–79.
Pugin, A., T. Larson, S. Sargent, J. McBride, and C. Bexfield (2004), Near-surface mapping using *SH*-wave and *P*-wave seismic land-streamer data acquisition in Illinois, U.S., *Leading Edge*, *23*(7), 677–682, doi:10.1190/1.1776740.
Pugin, A.-M., K. Brewer, T. Cartwright, S. Pullan, P. Didier, H. Crow, and J. Hunter (2013), Near surface *S*-wave seismic reflection profiling—New approaches and insights, *First Break*, *31*(2), 49–60, doi:10.3997/1365-2397.2013005.
Schacht, U., M. Regan, C. Boreham, and S. Sharma (2011), CO2CRC Otway Project—Soil gas baseline and assurance monitoring 2007–2010, *Energy Procedia*, *4*, 3346–3353, doi:10.1016/j.egypro.2011.02.256.
Schön, J. (2004), *Physical Properties of Rocks: Fundamentals and Principles of Petrophysics, Dev. in Petroleum Sci. Ser.*, Elsevier, New York.
Sheriff, R., and L. Geldart (1995), *Exploration Seismology*, vol. 1, 2nd ed., Cambridge Univ. Press, Cambridge, U. K.
Spencer, L., and F. La Pedalina (2006), Otway Basin Pilot Project, Naylor Field, Waarre formation unit C; reservoir static models, *Tech. Rep. CO2CRC Publ. Number RPT05-0123*, Coop. Res. Cent. for Greenhouse Gas Technol., Canberra, Australia.
State of Victoria (2015), Groundwater resource reports. [Available at http://www.depi.vic.gov.au/water/groundwater/groundwater-resource-reports], online; accessed: 30-March-2015.
Tickell, S., J. Edwards, and C. Abele (1992), Port Campbell embayment, *Tech. Rep. Australia Rep. 95*, Geol. Surv. of Victoria, Melbourne, Australia.
Vidal-Gilbert, S., E. Tenthorey, D. Dewhurst, J. Ennis-King, P. Van Ruth, and R. Hillis (2010), Geomechanical analysis of the Naylor Field, Otway Basin, Australia: Implications for CO_2 injection and storage, *Int. J. Greenhouse Gas Control*, *4*(5), 827–839, doi:10.1016/j.ijggc.2010.06.001.
Wald, D., and T. Allen (2007), Topographic slope as a proxy for seismic site conditions and amplification, *Bull. Seismol. Soc. Am.*, *97*(5), 1397–1395, doi:10.1785/0120060267.
Wallace, W., J. Dickinson, D. Moore, and M. Sandiford (2007), Late Neogene strandlines of southern Victoria: A unique record of eustasy and tectonics in southeast Australia, *Aust. J. Earth Sci.*, *52*(2), 279–297, doi:10.1080/08120090500139455.
Whiteley, R. (2012), Surface and borehole seismic imaging of soft-rock, karsteolianites at coastal engineering construction sites: Case studies from Australia, *Leading Edge*, *31*(1), 76–81, doi:10.1190/1.3679331.
Whitney, B., and J. Hengesh (2015), Geomorphological evidence of neotectonic deformation in the Carnarvon Basin, Western Australia, *Geomorphology*, *228*, 579–596, doi:10.1016/j.geomorph.2014.10.020.
Williamson, P., M. Swift, G. O'Brian, and D. Falvey (1990), Two-stage Early Cretaceous rifting of the Otway Basin margin of southeastern Australia: Implications for rifting of the Australian southern margin, *Geology*, *18*(1), 75–78.
Yilmaz, Ö. (2001), *Seismic Data Analysis; Volume I and II*, Soc. of Explor. Geophys., Tulsa, Okla.
Ziesch, J., C. M. Aruffo, D. C. Tanner, T. Beilecke, T. Dance, A. Henk, B. Weber, E. Tenthorey, A. Lippmann, and C. M. Krawczyk (2015), Geological structure of the CO2CRC Otway Project site, Australia: Fault kinematics based on quantitative 3-D seismic interpretation, *Basin Res.*, doi:10.1111/bre.12146, online first.